Nitrogen

Article

Gas-Phase Photocatalytic Transformations of Nitric Oxide Using Titanium Dioxide on Glass Fiber Mesh for Real-Scale Application

Marija Tomaš, Benjamin Radetić, Lucija Radetić, Paula Benjak and Ivana Grčić *

Department of Environmental Engineering, Faculty of Geotechnical Engineering, University of Zagreb, Hallerova Aleja 7, 42000 Varaždin, Croatia; mtomas@gfv.hr (M.T.); bradetic@gfv.hr (B.R.); lradetic@gfv.hr (L.R.); pbenjak@gfv.hr (P.B.)
* Correspondence: igrcic@gfv.hr

Abstract: In this paper, the degradation of nitric oxide (NO) in an annular laboratory reactor is presented. Preliminary experiments were performed in an annular reactor (AR) under simulated solar irradiation. Titanium dioxide (TiO_2 P25) was used as a photocatalyst and immobilized on glass fibers mesh (GM) by the sol–gel method prepared from commercially available materials. The aim of the experiments was to remove NO from the air stream. The initial rate constant of the NO photocatalytic degradation was recognized to follow mass-transfer-controlled first-order kinetics. The results confirmed the photocatalytic reduction of NO to molecular nitrogen (N_2) and oxidation to nitrate. Therefore, the preliminary results obtained in this work are used for the development of a computational fluid dynamics (CFD) model (COMSOL Multiphysics v6.2). CFD calculations provide a good basis for sizing reactors at the semi-pilot and pilot levels for both indoor and outdoor air purification systems.

Keywords: nitric oxide; titanium dioxide; photocatalysis; glass fibers mesh; CFD model; air purification

Citation: Tomaš, M.; Radetić, B.; Radetić, L.; Benjak, P.; Grčić, I. Gas-Phase Photocatalytic Transformations of Nitric Oxide Using Titanium Dioxide on Glass Fiber Mesh for Real-Scale Application. *Nitrogen* **2024**, *5*, 610–623. https://doi.org/10.3390/nitrogen5030041

Academic Editor: Shuguang Denge

Received: 31 May 2024
Revised: 4 July 2024
Accepted: 9 July 2024
Published: 10 July 2024

1. Introduction

Nitric oxide (NO) is a colorless, neurotoxic, odorless gas that is essentially insoluble in water [1]. It is released from various anthropogenic and natural sources, with diesel-powered vehicles and high-temperature combustion being significant contributors. The combination of NO and nitrogen dioxide (NO_2) constitutes nitrogen oxides (NO_x), which are major components of air pollution, particularly in urban areas. Regulations from organizations like the World Health Organization (WHO) and directives from entities such as the European Union (EU) aim to control air quality, but the concentrations of emitted pollutants like NO_x continue to rise in many urban areas. To address this challenge, the development and implementation of new ecological technologies for air purification are indeed necessary to meet regulatory requirements and reduce pollutant levels.

Solar photocatalysis represents an ecological technology for the degradation of airborne pollutants due to its process sustainability, low cost, long-term photostability, and non-selective degradation of pollutants. Photodegradation of nitric oxide has been widely researched using TiO_2 as a photocatalyst under UV light. Lasek et al., in their review, presented various catalysts for NO photo-decomposition and photo-oxidation processes [2]. Boyjoo et al. provided a review of photocatalytic oxidation for air treatment [3]. Compared to the removal of volatile organic compounds (VOCs), studies on nitrogen oxides in this field are less intensive. However, research on TiO_2-based studies of inorganic gas pollutants has similar efficiency as VOC removal [3]. Outdoor applications

based on commercial photocatalytic dispersion paints have shown successful results for NO removal under irradiation [4]. Dylla et al. provided important results for developing a reaction rate model for NO on photocatalytic pavements, offering a promising solution for remedying air pollution from automobile sources [5]. Maggos et al. tested TiO_2-containing paints, which resulted in 74% removal efficiency of NO on mineral silicate paint and 91% on styrene acrylic paint [6]. TiO_2 P25 is commercially available, non-toxic, and photochemically and biologically stable, with high photoactivity and mineralization efficiency composed of anatase and rutile crystallites (crystalline content of 70–80% anatase and 20–30% rutile) [1,3,4,7]. Bianchi et al. compared the photocatalytic performances of pigmentary powdered TiO_2 (crystalline content of 100% anatase) and P25 by Evonik (crystalline content of 75% anatase and 25% rutile) in NO_x degradation. P25 resulted in the highest efficiency and the highest amount of hydroxyl species reaching NO_x degradation after 120 min [8]. Zouzelka and Rathousky applied a coating of TiO_2 P25 on concrete walls along a busy thoroughfare in Prague [9]. The photocatalytic coating maintained its ability to abate NO_x pollutants in the air even two years after application [9]. In the field of air purification, TiO_2 immobilization can include various methods such as sol–gel, thermal spraying, solvent deposition, electrophoresis, and chemical and physical vapor deposition. Wood et al., through their review, determined that the sol–gel method had the highest normalized removal rate for NO_x [10]. The band gap of photocatalysts plays an important role in forming of electron–hole pairs. TiO_2 is characterized by a large band gap energy (3.2 eV) which limits its application under natural solar light or artificial visible light.

When the irradiating light has higher energy than the photocatalyst's band gap, electrons (e^-) in the conduction band (CB) are forming, thus leaving empty space in the valence band (VB) resulting in holes (h^+) [11]:

$$\mathrm{TiO_2} + h\nu \rightarrow e^- + h^+, \quad (1)$$

These holes have powerful oxidation potential and, with electrons in the CB, cause the formation of radical hydroxyl species (OH^-) and oxygen (O_2^-) [11]:

$$\mathrm{OH^-} + h^+ \rightarrow \mathrm{OH} \quad (2)$$

$$\mathrm{O_2} + e^- \rightarrow \cdot \mathrm{O_2^-} \quad (3)$$

The radical species formed participate in further oxidation and reduction reactions leading to the degradation of nitrogen oxides [12]:

$$\mathrm{NO} + \cdot \mathrm{O_2} \rightarrow \mathrm{NO_3^-} \quad (4)$$

$$\cdot \mathrm{OH} + \mathrm{NO} \rightarrow \mathrm{HNO_2} \quad (5)$$

$$\mathrm{HNO_2} + \cdot \mathrm{HO} \rightarrow \mathrm{HNO_3} \quad (6)$$

Adsorbed nitric oxides on the surface of photocatalytic material also follow alternative pathways in which the reduction ability of photocatalysis is used to form nitrogen (N_2) [3,13,14]:

$$\mathrm{NO_{ads}} + e^- \rightarrow \mathrm{N_{ads}} + \mathrm{O_{ads}} \quad (7)$$

$$\mathrm{NO_{ads}} + \mathrm{N_{ads}} \rightarrow \mathrm{N_2O_{ads}} \quad (8)$$

$$\mathrm{NO_{ads}} + \mathrm{O_{ads}} \rightarrow \mathrm{NO_{2,ads}} \quad (9)$$

$$2\mathrm{O_{ads}} \rightarrow \mathrm{O_{2,ads}} \quad (10)$$

$$2N_{ads} \rightarrow N_{2(g)} \quad (11)$$

$$2NO_{ads} \rightarrow O_{2(g)} + N_{2(g)} \quad (12)$$

$$N_2O_{ads} \rightarrow O_{ads} + N_{2(g)} \quad (13)$$

In the present work, photocatalytic oxidation experiments were provided using an annular reactor for the purification of air polluted with NO. This reactor geometry is widely utilized in commercial photoreactors due to its proven efficiency in solar photocatalysis applications. The widely researched sol–gel method for TiO_2 immobilization was used on a glass fiber mesh. A reactor system can be easily scaled up and installed as a ventilation outlet or exhaust. Therefore, as the initial step in developing a computational fluid dynamics (CFD) model, experimental laboratory results were obtained to provide the photocatalytic reaction kinetics of NO reduction. CFD models are important for understanding the expected significance of NO reduction. The presented model provides solutions for scaling up the reactor system. Additionally, improving this model in the future could enable the evaluation of photocatalysis as a potential pollution reduction strategy.

2. Materials and Methods

2.1. Photocatalytic Material

The photocatalyst TiO_2 P25 (Evonik, Aeroxide®, Essen, Germany) was immobilized on the surface of a glass fiber mesh (GM) according to the procedure described previously in [15,16]. GM is a fabric composed entirely of glass fibers with a density of 480 g/m^2 and dimensions of 200 × 450 mm, corresponding to the annular reactor (AR). TiO_2 P25 was attached to the carrier using the sol–gel method, which includes acetic acid (Kemika, Zagreb, Croatia), tetraethoxysilane (TEOS) (Sigma-Aldrich, Steinheim, Germany), 96% ethanol p.a., deionized water, and 10 M NaOH [15–17]. The photocatalyst has an elementary particle size of 30 nm, a BET surface area of 56 m^2/g, and a crystalline content of 75% anatase and 25% rutile. A suspension for immobilizing TiO_2 P25 was prepared through several steps, beginning with the preparation of the initial mixture, which involved mixing and stirring water, ethanol, and TiO_2. The pH adjustment was achieved by adding acetic acid slowly until the pH reached 1.5. The mixture was stirred for 15 min. Then, sonication with an ultrasonic probe was performed for 2 min at 30 W and 44 kHz. In the next step, TEOS was added, followed by stirring for an additional hour at 50 °C. The final step involved immersing a glass fiber mesh in the prepared solution and drying it at 70 °C. This procedure was iterated five times to achieve five layers of TiO_2. Before the initial immersion, the GM underwent treatment with a 10 M NaOH solution for 5 min, followed by rinsing with demineralized water to enhance surface adhesion. The material characterization and optical properties were discussed in our recent publication [15–17]. As outlined in previous studies, the TiO_2 film supported on the GM exhibited flexibility, durability, and the capability to be easily rolled into a cylinder for application in an AR. Before and after TiO_2 immobilization, the GMs were weighed, enabling the calculation of the TiO_2 proportion in the immobilized layer at 77.6 wt.% based on mass balance. The average mass of the film immobilized on the GM surface was determined to be 0.0017 ± 0.0001 g/cm^2. Additionally, the thickness of the photocatalytic layer (GM + TiO_2 film) was measured at 3.4 ± 0.2 mm.

2.2. Photocatalytic Setups

Photocatalytic setups contain a NO gas bottle (c = 50 ppm, N_2 balance, Linde, Prague, Czech Republic), an annular reactor, an air pump, an Erlenmeyer flask filled with distilled water, and a gas wash bottle (Figure 1).

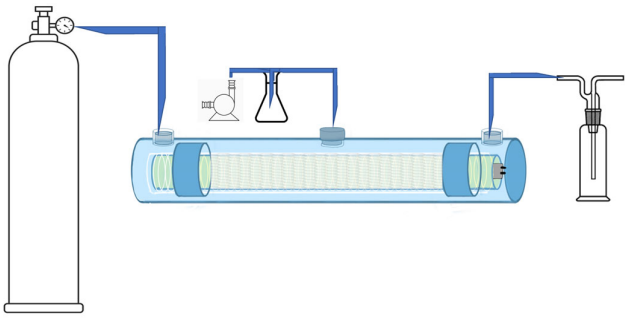

Figure 1. Schematic of annular reactor setup.

An air pump (Marina100, HAGEN Deutschland GmbH & Company KG, Holm, Germany) with a maximum flow rate of 85 L/h was attached to an Erlenmeyer flask, which was connected to the second AR opening with tubes. The annular reactor was cylindrical and made of glass. In the center of the annular reaction area, a full-spectrum linear fluorescent light bulb (Narva BIO vital® LT T5 24 W/958, 549 mm long, NARVA Lichtquellen GmbH + Co. KG, Brand-Erbisdorf, Germany) was placed [18]. The incident intensities of UVA and UVB were measured using a UVP UVX radiometer (Analytik Jena, Upland, CA, USA), resulting in 1.73 mW/cm^2 for UVA and 1.49 mW/cm^2 for UVB [16]. The spectral characteristics of the radiation source used match the spectrum of solar radiation with a nominal luminous flux of 1400 lm. The geometry of the reactor is as follows: diameter D = 60 mm, length L = 600 mm, the outer radius is R = 2.7 cm, the inner radius is R_{in} = 2.0 cm, and the reactor volume is 7.83 × 10^{-4} m^3. The photocatalytic film, mounted on a glass fiber mesh, was rolled into a cylinder and affixed to the outer wall of the reactor within the annular reaction space. The annular reactor had three openings: the first at the beginning of the reactor, serving as an inlet; the second in the middle, used for introducing moisture; and the third at the end of the cylinder, functioning as an outlet. Measurements were taken at both the inlet and outlet of the reactor. Monitoring of the gases carbon monoxide (CO; 0–10,000 ppm), carbon dioxide (CO_2; 0–50 vol.%), NO (0–4000 ppm), NO_2 (0–500 ppm), hydrocarbon (HC; natural gas 100–40,000 ppm; propane 100–21,000 ppm; butane 100–18,000 ppm), hydrogen sulfide (H_2S; 0–300 ppm) was conducted using a gas analyzer Testo 350 (Testo SE & Co. KGaA, Lenzkirch, Germany). To detect possible photoreaction products, nitrate anions (HNO_3/NO^{3-}) were measured using Quantofix nitrate test strips (nitrate 10–500 mg/L; nitrite 1–80 mg/L; MACHEREY-NAGEL GmbH & Co. KG, Düren, Germany). The reactor was upgraded with a simple Arduino-based analytical platform for continuous temperature and humidity monitoring.

The first set of experiments was conducted without the photocatalyst under irradiation to establish the outlet's baseline NO levels and the corresponding residence time. The second set of experiments involved the use of glass fibers with immobilized TiO_2 performed in the dark. The experiment of photocatalytic oxidation involves exposing the setup to artificial light with certain UV irradiation, which works in synergy with the photocatalyst to act on NO molecules in the air stream. Experiments under irradiation began with the system being equilibrated in darkness for 60 min. Each experiment lasted for a duration of 2.5 h.

To demonstrate the efficiency of the previously described annular reactor for NO decomposition, the computational program COMSOL Multiphysics v6.2 was utilized. The AR model in this CFD software v6.2 enabled the visualization of data for laminar flows and the solving of computational simulations. By using Computational Fluid Dynamics (CFD), it is possible to obtain satisfactory fluid flow simulations and solve the Radiation Transport Equation (RTE). The aim is to develop a mathematical model of a reactor for photocatalytic degradation using a scaling-up methodology, enabling the construction of reactors on a larger scale while simulating their behavior. This approach leads to optimizing the reactor itself for real-world applications. The scaling-up methodology

involves deriving a chemical kinetic expression that corresponds to the photocatalytic degradation of NO in the reactor. When scaling the reactor, it is necessary to use the same kinetic reaction model as in laboratory experiments. In doing so, optimizing input parameters is necessary to ensure they are in the appropriate ratio with the new (pilot) reactor and to validate the obtained results. For photocatalytic reactors, it is necessary to model the hydrodynamic conditions that are influenced by the free flow through the reaction system.

In laminar flow achieved in the CFD software, the Navier–Stokes equation is used to calculate the hydrodynamic characteristics of single-phase photoreactor systems:

$$\rho\frac{\partial u}{\partial t} + \rho(u \times \nabla)u \ = \nabla\left[-pI + \mu\left(\nabla u + (\nabla u)^T - \frac{2}{3}\mu(\nabla \times \mathrm{u})\right)\right] + F, \quad (14)$$

$$\rho\nabla \ \times \ (u) = 0, \quad (15)$$

where u is the fluid velocity, p is the fluid pressure, ρ is the fluid density and μ is the fluid dynamic viscosity [19]. During simulation, the Navier–Stokes equation is solved using no-slip boundary conditions and calculates the pressure and fluid velocity in the model. The model is provided with the density ρ of air and the initial air flow velocity u. Solving the equation for a specific set of boundary conditions (such as inlets, outlets, and walls) predicts the liquid velocity and pressure in the given model geometry.

3. Results

3.1. Results of Photocatalytic Transformation of Nitric Oxide

Experimental results in an annular reactor, shown in Figure 2, combine the results obtained under conditions without and with exposure to an artificial radiation source in an empty reactor space and using a photocatalyst on a glass fiber mesh (GM).

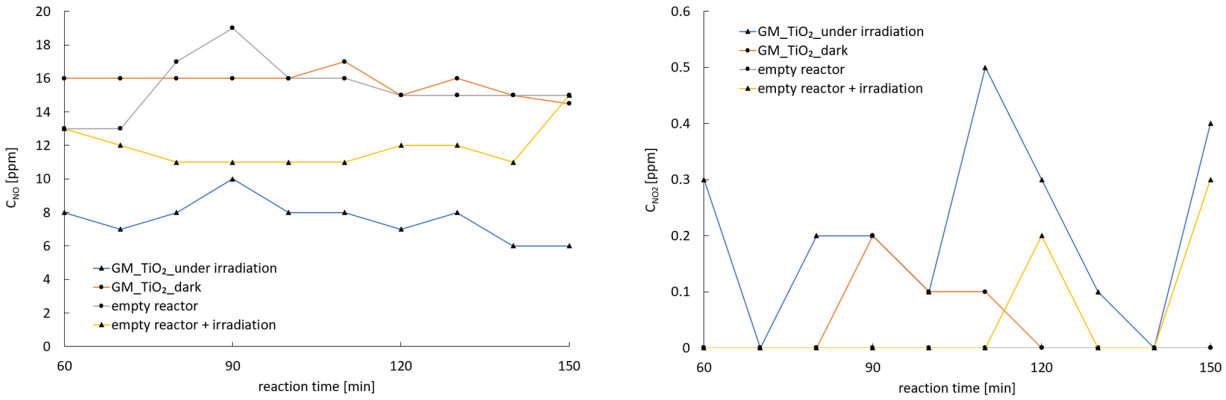

(**a**) (**b**)

Figure 2. Measured NO (**a**) and NO_2 (**b**) concentration at the outlet: comparison of NO and NO_2 trends in an empty reactor with and without irradiation and during the adsorption experiments (GM_TiO_2_dark) and photocatalytic experiments (GM_TiO_2_under irradiation).

The adsorption experiment (GM_TiO_2_dark) was conducted on the surface of a supported photocatalytic film in the dark to test the adsorption of nitric oxide (NO). All measurements were performed after 60 min when a steady state was well achieved. It is noticeable that the concentration of NO changes insignificantly due to the presence of the photocatalyst in the reactor, which indicates the negligible adsorption of NO on the GM_TiO_2 surface. Considering the NO trends in the outlet shown in Figure 2a, it is obvious that NO undergoes transformation under irradiation, possibly due to the formation of radicals upon absorbing the incident irradiation by the NO molecule. The results of monitoring the NO_2 concentration in the outlet suggest that photocatalysis over

the supported TiO_2 directs the NO transformation towards NO_2. In the photocatalytic experiments (GM_TiO_2_under irradiation), NO transformation was observed, resulting in an expected almost uniform concentration in the outlet. The variations in NO_2 concentrations in the outlet suggest a more complex reaction mechanism than the straightforward oxidation of NO to NO_2. A complex mechanism was also suggested in the literature [20]. The measured percentage of N_2 in the outlet was slightly higher, also suggesting the reduction of NO over the irradiated photocatalyst. No formation of N_2O occurred during the experiment. The concentrations of NO_2^- and NO_3^- in the rinse water were measured using Quantofix test strips. Results showed coloring for NO_3^- in the range of 10–25 mg/L.

Arduino-based analytical platforms for continuous monitoring of the temperature and humidity measured relative humidity at a range of 70–80% and temperature at a range of 20–22 °C in each experiment. In the photocatalytic experiment, CO concentrations ranging from 1 to 3 ppm were detected, probably due to incomplete oxidation of organic components of the photocatalytic film.

For a clear quantitative comparison, the simple kinetic model was employed to describe the initial rates of photocatalytic degradation of NO, which followed mass-transfer-controlled first-order kinetics due to a low concentration of target pollutants.

The photocatalytic degradation of nitric oxide can be simulated as a pseudo-first-order reaction:

$$\ln\left(\frac{C}{C_0}\right) = -k\tau \quad (16)$$

where k is the reaction rate constant of NO under photocatalytic degradation, C is the concentration of NO measured at outlet and C_0 is the initial concentration [21–23].

The relative changes in the NO and NO_2 concentration during the photocatalytic degradation of NO versus exposure time are shown in Figure 3.

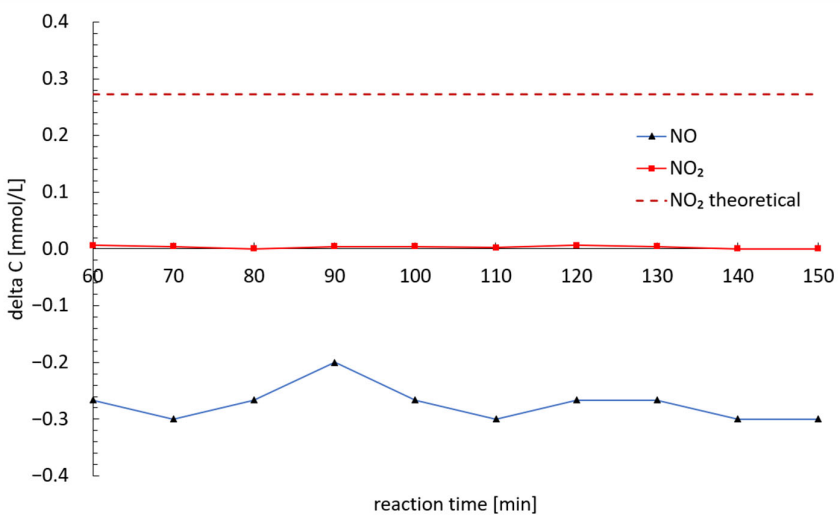

Figure 3. Relative changes in NO and NO_2 concentration during photocatalytic transformations in AR reactor; difference was obtained taking into account measured concentrations during adsorption experiments (GM_TiO_2_dark) and photocatalytic experiments (GM_TiO_2_under irradiation).

Figure 3 gives a better representation of continuous NO transformation towards different products. The determined reaction rate constant was k = 0.0984 min^{-1}. Mass balance calculations show that during photocatalytic experiments 11.47 mmol/L of nitrogen species (NO, NO_2) flow through the AR in total, giving a theoretical concentration of 1.4 g/L of NO_3^- in the rinse. Calculations based on only the NO_2 mass

balance give the theoretical concentration of 25.2 mg/L of NO_3^- in the rinse which corresponds with the highest experimental value of NO_3^- in the rinse obtained.

3.2. CFD Modelling of Photocatalytic Annular Reactor

The computer simulation of nitric oxide (NO) decomposition enabled a visual representation of the obtained results using COMSOL Multiphysics software. The reactor model (Figure 4) is set up as described in the Discussion and consists of built geometry, a fluid flow model, a radiation model, a model of chemical reactions, and species transport through the reactor. The main purpose of the computer model was to compare it with experimental results obtained in a laboratory to test its accuracy for scaling and optimizing future reactors for use in real systems. This approach also facilitates identifying and overcoming obstacles that affect photocatalytic oxidation. The duration of all simulations was 150 min, or 9000 s, as in the case of measurements. In the simulation in COMSOL Multiphysics shown, the input concentration value of 2.045×10^{-6} mol/L was used, considering atmospheric pressure (101,325 Pa) and an average temperature inside the reaction volume (293.15 K).

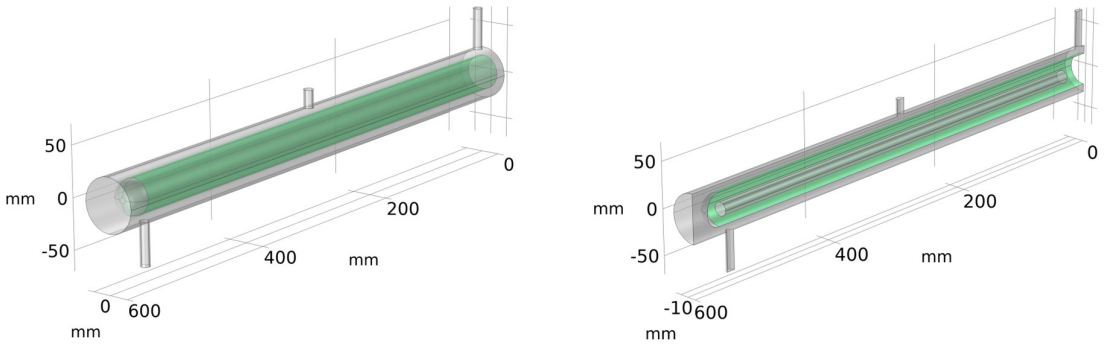

Figure 4. Representation of the modeled annular reactor with highlighted surface where reactions occur: (**a**) complete reactor; (**b**) half of the reactor used in simulation calculations.

The streamlines and steady-state velocity field, simulated for a 1 L/min inlet flow rate using a stationary solver, can be seen in Figure 5. The inlet and outlet had the highest velocities.

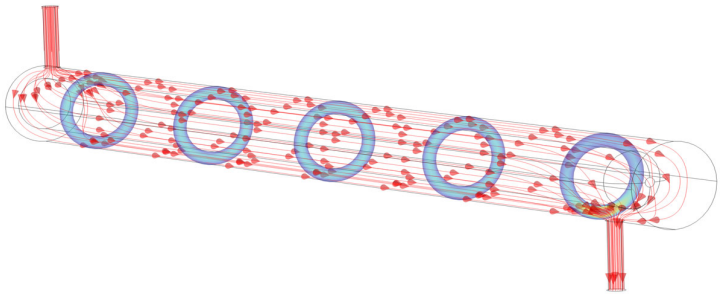

Figure 5. Velocity streamlines with fluid flow at a flow rate of 1 L/min.

In Figure 6, the irradiance distribution is plotted to demonstrate a uniform distribution along the surface reaction area (TiO_2-coated walls). It is clear that the coated surface receives light and provides valuable insight into irradiance distribution, which can be difficult to measure conventionally. Additionally, these data can be used to optimize the reactor design by adjusting the position of the emission source (lamp), increasing the power, or varying the layer coating thickness.

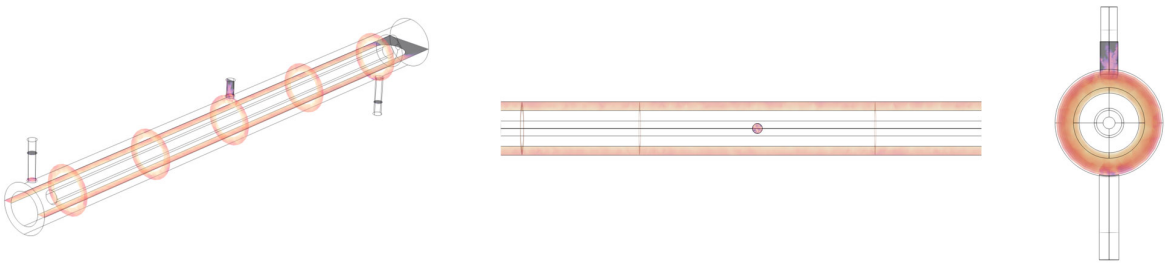

(**a**) (**b**) (**c**)

Figure 6. Visual representations of the artificial light under certain UV irradiation distribution in the annular reactor: (**a**) 3D representation; (**b**) representation in the xy-plane; (**c**) representation in the yz-plane.

The stated results coincide with the results obtained in the model in the COMSOL Multiphysics interface, where the concentration of nitric oxide (NO) at the outlet is expressed in the amount of 2.45 × 10^{-7} mol/L. The agreement between the laboratory test results and the model suggests that the model accurately represents the fundamental processes of photocatalytic oxidation that are studied in this case, thus confirming the effectiveness and prediction of the model of photocatalytic oxidation of NO. In order to determine whether the length of the pipe (reactor) has an influence on NO decomposition, a simulation was made with an increased length of the pipe, the results of which are shown in Figure 7. As can be seen from the results, there was a minor decrease in the NO concentration in the reactor compared to the input concentration. The above represents a difference compared to the results obtained by simulating a longer reactor tube and the original length and indicates that the extended retention time of pollutants in the reactor really provides more opportunities for photocatalytic decomposition of NO. Therefore, scaling the length of the reactor is proving to be a key factor for the use of this technology.

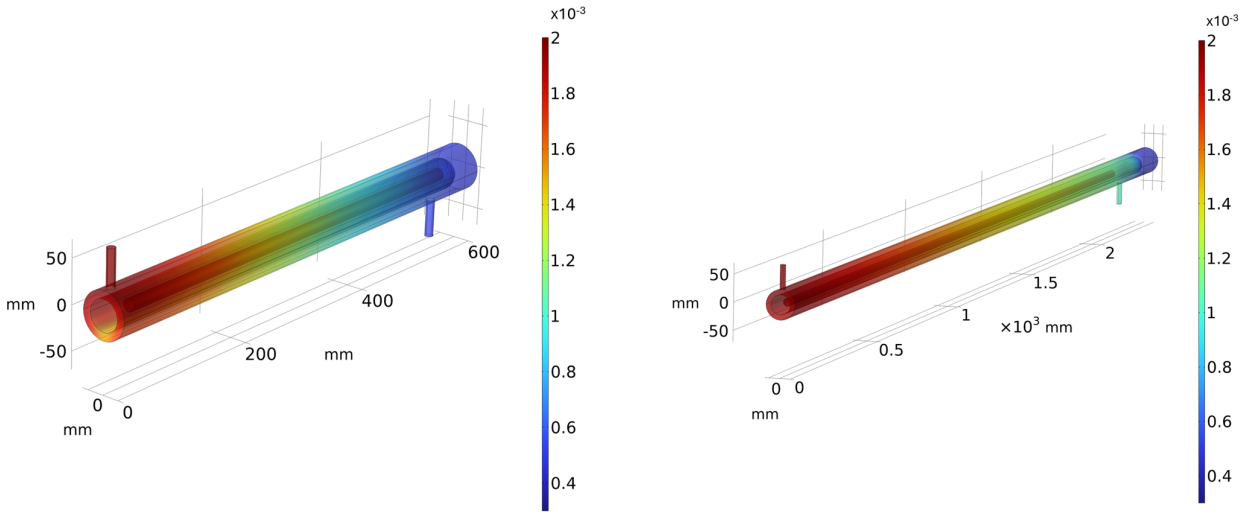

(**a**) (**b**)

Figure 7. Simulated concentration profile of NO at time step t = 9000 s at inlet concentration of 2.045 10^{-6} mol/L in (**a**) original reactor L = 600 mm; (**b**) prolongated reactor L = 2400 mm.

Since the stated and provided results successfully replicate the test results, the built model of the photocatalytic reactor can serve as a solid foundation for future system optimization.

4. Discussion

Photocatalytic heterogeneous reactions follow the Langmuir–Hinshelwood mechanism (L-H), which involves the reactant molecules first being adsorbed onto the catalytic surface before participating in the reaction. At low reactant concentrations, typical of indoor air pollution, the Langmuir–Hinshelwood (L-H) model simplifies to a pseudo-first-order expression [21–24].

Reaction kinetics provide insight into reaction rates and mechanisms, commonly expressed using the power law:

$$-\frac{dC}{d\tau} = k[C]^n \quad (17)$$

where k is the rate constant and n is the reaction order [25].

Introducing moisture in the annular reactor, the photogenerated holes can also oxidize water molecules to produce many hydroxyl radicals (•OH) for oxidizing NO molecules. Li et al. investigated photocatalytic performance for the removal of NO gas on Bi_2WO_6 samples. The Bi_2WO_6 samples with the highest BET surface area (37 m^2/g) resulted from the highest initial rate constant of 0.0385 min^{-1} [22]. Ai et al. synthesized BiOBr microspheres and bulk powder. Photocatalytic removal of NO under UV-visible irradiation resulted from k = 0.0841 min^{-1} for microspheres and 0.0167 min^{-1} for bulk powder [24]. Under visible light irradiation, BiOBr microspheres reached k = 0.0614 min^{-1} and k = 0.0094 min^{-1}. Based on this research, glass fiber mesh with immobilized TiO_2 in an annular reactor resulted in an initial rate constant of k = 0.0984 min^{-1}. Degussa TiO_2 P25 photocatalysts for photocatalytic decomposition and reduction of NO were investigated by Bowering et al. Scientists concluded that NO will react to form N_2 and N_2O with higher selectivity for N_2 formation when on a titanium surface that is rich in hydroxyl groups [14]. Additionally, in the presence of CO, the selectivity of the reaction for N_2 formation was higher [14]. In this work, all measured inlet concentrations of NO_x were the same as the NO concentration. Previous results indicated that NO reacted to form NO_2 but the measured concentrations were below expected levels, confirming the main reaction mechanism of NO reduction towards N_2. The oxidation pathway led to the formation of nitrates which were measured in the rinse. The concentration of NO_3^- in the rinse after the photocatalytic experiments was also below the calculated theoretical value based on NO_2 concentrations, suggesting that the formation of other possible reaction products (N_2O_4 dimer and others) is negligible. Zouzelka and Rathousky investigated the photocatalytic activity of the commercial product containing TiO_2 P25 by Evonik with regard to NO and NO_2 abatement where the final product of photocatalytic oxidation captured on the photocatalytic surface of the samples was exclusively nitrate, while no nitrites were retained [9]. Taking these results into account, it is clear why only nitrates were detected in our case.

According to Fermoso et al., the application of solar photocatalysis for indoor air treatment requires the optimization of by-product non-generation and the maximization of the photocatalytic configuration through increased roughness, porosity, and abrasion resistance [26]. Additionally, it is necessary to have excellent geometric surface area arrangements, proper illumination of photoactive sites, and optimum immobilization of the photocatalysts with regeneration capability [26]. Glass fiber mesh with TiO_2 as a photocatalyst showed good properties based on the material characterization and optical properties presented in our recent paper [15,16]. This photocatalytic film achieved photocatalytic degradation of ammonia in the air stream, and dihydroxybenzenes, 17β-estradiol, enrofloxacin, and 1H-benzotriazole as common waterborne pollutants [15,16,27].

Geng et al. provided a critical review of the main challenges in photocatalytic technology for air purification [28]. So far, TiO_2 is the most widely used photocatalyst in outdoor applications. Chen and co-workers immobilized TiO_2 (anatase) on the surface of cement and asphalt roads, aiming for the removal of NO_x [29,30]. In their review, Geng et al. concluded that the main challenge for outdoor applications is to develop high-

performance, visible-light-driven photocatalysts that balance the efficiency of visible light absorption and oxidation capacity [28]. TiO_2 P25 has low activity under visible light irradiation, although it shows good purification efficiency. In this work, the purification system includes an annular reactor using TiO_2 P25 on a glass fiber mesh. Annular reactors are recommended for indoor applications because they are not designed for high air permeability [31]. On the other hand, to improve our photocatalytic material for outdoor applications, we should expand the visible light response of TiO_2 P25. This can be achieved through various procedures, such as doping TiO_2 with non-metal or metal compounds, combining TiO_2 with other semiconductors through vapor deposition, and incorporating cations and anions into the TiO_2 structure. Duan et al. used Ag nanoclusters on the surface of TiO_2 P25 for the photocatalytic removal of NO, resulting in a purification rate of 63% [32]. Jiang et al. prepared ceramic tiles by coating them with a layer of TiO_2 tri-doped with N, F, and Fe ions using the sol–gel method. The ceramic tiles were active under visible light and achieved a 44% efficiency in removing NO [33]. Another bottleneck with P25 is its powder structure, which can be easily blown out during the reaction process [28]. The sol–gel method described in this work provides a good solution for P25 immobilization. TiO_2 P25 on glass fiber mesh can be easily implemented in industrial production considering safety conditions, low cost, and photocatalytic efficiency.

When modeling a reactor, it is necessary to implement mathematical models such as the radiation absorption-scattering model, radiation emission model, kinetic model, and fluid dynamics model [34,35]. For the modeling of the fluid flow, pollutant transport, and RTE equation, the commercial CFD software COMSOL Multiphysics 6.2 was used. The CFD model was solved in three consecutive steps. First, the model geometry was built for the annular reactor with the reactor dimensions, volume, and lamp described in the Materials and Methods. The flow field across the computing domain was then obtained by solving the equations of conservation of mass and momentum. Subsequently, the radiation field was obtained by solving the RTE. This approach to the problem reduces the computation time and steadies the result [36,37]. The Radiation Transport Equation (RTE) depends on the specific geometry of the photocatalytic reactor and the type of light source. The applied RTE method is the Discrete Ordinates Method (DO), which has been recognized in previous research as accurate and flexible [34,38]. There are three primary methods for illuminating photocatalytic reactors: (1) the lamp shining directly on the reactors from a distance, as in the case of immobilized reactors; (2) immersing the lamp directly into the reaction space, as in the case of slurry annular reactors; and (3) using reflecting devices, such as parabolic and elliptical reflectors, to irradiate the reactor with direct and reflected radiation. Lamps can emit light either diffusely or specularly. However, due to its simplicity and high degree of accuracy, the specular model has been deemed satisfactory for UV lamps in general. It is recommended to measure experimentally the radiation intensity using a detector near the lamp surface to obtain accurate results [39]. By resolving the radiative (photon) transfer equation (RTE) for the heterogeneous system, the surface irradiation inside the reactor was evaluated.

The RTE for monochromatic radiation is described as follows [35,39–41]:

$$\frac{dL(r,s)}{dz} + (\kappa + \sigma)L(r,s) = j^e(r) + \frac{\sigma}{4\pi}\int_{4\pi} L(r,s')p(s' \to s)d\Omega' \quad (18)$$

where L is photon radiance, r is the position vector, s is the propagation vector, z is the path length, κ is the absorption coefficient, σ is the scattering coefficient, p is the phase function for the scattering of photons, and Ω' is the solid angle about the scattering vector s'. The integro-differential form of the RTE is converted into an algebraic system of equations that may be solved computationally by using the discrete ordinate method (DO). The radiation field is discretized into several distinct directions in the DO method, and the RTE is expressed and solved independently for each direction. When it comes to radiation, the DO method is recognized for providing the most precise results for both suspended and immobilized systems [42,43]. As part of the boundary conditions definition,

all the incident radiation reaching the TiO_2-coated walls was assumed to be absorbed; therefore, no radiation was reflected or transmitted. In immobilized reactors, near-wall treatment can be properly modeled in CFD by discretizing the domain close to the wall into a sufficiently large number of control volumes or control cells. Since the flow along the walls is laminar, the simple standard wall function with no slip shear conditions can be used [39]. No radiation was reflected or transmitted since it was believed that all incident radiation that reached the TiO_2-coated walls would be absorbed as part of the boundary conditions definition. By discretizing the area near the wall into an adequate number of control volumes or control cells, near-wall treatment in immobilized reactors can be accurately predicted in CFD. It is possible to apply the simple standard wall function with no slip conditions since the flow along the walls is laminar [35].

Fluid flow simulations are among the first steps in photocatalytic reactor modeling. The hydrodynamics of single-phase photoreactor systems can be computed using the traditional Navier–Stokes equations [39]. Since the photocatalyst in the model was immobilized on the wall of the photoreactor, it was assumed that the fluid was Newtonian, incompressible, isothermal, non-reactive, with constant physical properties [35]. For pollutant transport through the reactor (NO), a laminar airflow model was used. At the inlet, a volumetric flow rate of 1 L/min was specified, while, for the outlet, a constant atmospheric pressure was defined.

By resolving the governing equations of momentum and mass continuity, a steady-state solution was obtained [37]:

$$\rho(u\nabla)u = \nabla(-pI + (\mu + \mu t)(\nabla u + \nabla u^T)) \quad (19)$$

$$\rho\nabla(u) = 0 \quad (20)$$

where ρ is the air density, u is the velocity vector, I is an identity matrix, p is the pressure, μ is the dynamic viscosity, and μt is the eddy viscosity which equals zero in the case of laminar flow.

The concentration of NO in the bulk phase was solved with the convection–diffusion equation by coupling the velocity field of the previous stationary study [37]:

$$(-D\nabla C_{NO}) + u\nabla C_{NO} = 0 \quad (21)$$

where D is the diffusion coefficient of NO in the air, C_{NO} is the bulk concentration of NO, and u is the velocity field vector.

The adsorption of organic contaminants onto the TiO_2 catalyst surface is a crucial process in photocatalysis. It is necessary to model simultaneous adsorption/desorption at the surface. Therefore, a new species, NO_{ads}, was added. The boundary condition was determined by considering the surface reaction occurring at the walls coated with a photocatalyst.

The process of adsorption and desorption was modeled as a flux from bulk NO to the surface of TiO_2 [37,44,45]:

$$-n(-D\nabla C_{NO}) = -R_{ads} + R_{des} \quad (22)$$

where n is the normal vector of the boundary pointing towards the bulk phase. R_{ads} and R_{des} are defined as the species flux towards and outwards from the boundary.

Due to the photocatalytic reaction, one additional sink term (R_{pco}) was added to describe the loss of adsorbed molecules [37,44,45]:

$$\frac{\partial C_{NO,ads}}{\partial t} = R_{ads} - R_{des} - R_{pco} \quad (23)$$

where R_{pco} is the photocatalytic reaction rate expressed as a first-order reaction rate influenced by irradiation [37,44,45]:

$$R_{pco} = k_{pco}(I)C_{NO,ads} \quad (24)$$

The detailed reaction and transport mechanism can be found in [37,44,45].

The intrinsic kinetics are based on photocatalytic reactions and introduce factors arising from radiation conditions, the amount of photocatalyst, and the initial concentration of the compound [46]. In the radiation model, the primary parameter is determining the effect of radiation absorption on the rate of the photocatalytic reaction [46]. Simultaneously, the presence of absorption and scattering is crucial for radiation modeling (RTE).

5. Conclusions

The presented paper suggests that the photocatalytic transformation of NO in humid air follows two reaction pathways: reduction to N_2 and oxidation to nitrates. Understanding the kinetic models of photocatalytic oxidation is crucial for optimizing experimental conditions and designing large-scale photocatalytic reactors. Although annular reactors are not designed for high air permeability, and therefore cannot be commercialized for outdoor air purification, CFD can provide solutions to implementing this type of air purification reactor.

Author Contributions: Conceptualization, M.T., L.R., and I.G.; methodology, M.T., P.B., and B.R.; software, B.R.; validation, I.G.; formal analysis, M.T. and B.R.; investigation, M.T.; resources, I.G.; data curation, M.T.; writing—original draft preparation, M.T. and B.R.; writing—review and editing, I.G., P.B., and L.R.; visualization, M.T. and B.R.; supervision, I.G. and L.R.; project administration, I.G.; funding acquisition, I.G. All authors have read and agreed to the published version of the manuscript.

Funding: This research was funded by the project, "Recycling rubber & solar photocatalysis: ecological innovation for passive air and health protection", supported by the European Regional Development Fund, KK.01.1.1.07.0058.

Data Availability Statement: All the necessary data are provided in the present article.

Acknowledgments: This work has been supported by the Virtulab project (KK.01.1.1.02.0022) and was co-funded by the European Regional Development Fund.

Conflicts of Interest: The authors declare no conflicts of interest. The funders had no role in the design of the study; in the collection, analyses, or interpretation of data; in the writing of the manuscript; or in the decision to publish the results.

References

1. Vallero, D. *Fundamentals of Air Pollution*, 5th ed.; Academic Press: Cambridge, MA, USA, 2019; ISBN 9788578110796.
2. Lasek, J.; Yu, Y.H.; Wu, J.C.S. Removal of NOx by Photocatalytic Processes. *J. Photochem. Photobiol. C Photochem. Rev.* **2013**, *14*, 29–52. https://doi.org/10.1016/j.jphotochemrev.2012.08.002.
3. Boyjoo, Y.; Sun, H.; Liu, J.; Pareek, V.K.; Wang, S. A Review on Photocatalysis for Air Treatment: From Catalyst Development to Reactor Design. *Chem. Eng. J.* **2017**, *310*, 537–559. https://doi.org/10.1016/j.cej.2016.06.090.
4. Laufs, S.; Burgeth, G.; Duttlinger, W.; Kurtenbach, R.; Maban, M.; Thomas, C.; Wiesen, P.; Kleffmann, J. Conversion of Nitrogen Oxides on Commercial Photocatalytic Dispersion Paints. *Atmos. Environ.* **2010**, *44*, 2341–2349. https://doi.org/10.1016/j.atmosenv.2010.03.038.
5. Dylla, H.; Hassan, M.M.; Thibodeaux, L.J. Kinetic Study of Photocatalytic Degradation of Nitrogen Monoxide with Titanium Dioxide Nanoparticles in Concrete Pavements. *Transp. Res. Rec.* **2014**, *2441*, 38–45. https://doi.org/10.3141/2441-06.
6. Maggos, T.; Bartzis, J.G.; Leva, P.; Kotzias, D. Application of Photocatalytic Technology for NOx Removal. *Appl. Phys. A Mater. Sci. Process.* **2007**, *89*, 81–84. https://doi.org/10.1007/s00339-007-4033-6.
7. Ohtani, B.; Prieto-Mahaney, O.O.; Li, D.; Abe, R. What Is Degussa (Evonic) P25? Crystalline Composition Analysis, Reconstruction from Isolated Pure Particles and Photocatalytic Activity Test. *J. Photochem. Photobiol. A Chem.* **2010**, *216*, 179–182. https://doi.org/10.1016/j.jphotochem.2010.07.024.
8. Bianchi, C.L.; Pirola, C.; Galli, F.; Cerrato, G.; Morandi, S.; Capucci, V. Pigmentary TiO_2: A Challenge for Its Use as Photocatalyst in NOx Air Purification. *Chem. Eng. J.* **2015**, *261*, 76–82. https://doi.org/10.1016/j.cej.2014.03.078.
9. Zouzelka, R.; Rathousky, J. Photocatalytic Abatement of NOx Pollutants in the Air Using Commercial Functional Coating with Porous Morphology. *Appl. Catal. B Environ.* **2017**, *217*, 466–476. https://doi.org/10.1016/j.apcatb.2017.06.009.

10. Wood, D.; Shaw, S.; Cawte, T.; Shanen, E.; Van Heyst, B. An Overview of Photocatalyst Immobilization Methods for Air Pollution Remediation. *Chem. Eng. J.* **2020**, *391*, 123490. https://doi.org/10.1016/j.cej.2019.123490.
11. Schneider, J.; Bahnemann, D.; Ye, J.; Li Puma, G.; Dionysiou, D.D. (Eds.) *Photocatalysis Fundamentals and Perspectives*; The Royal Society of Chemistry: Cambridge, UK, 2016; ISBN 9781782620419.
12. Li, S.; Chen, L.; Ma, Z.; Li, G.; Zhang, D. Research Progress on Photocatalytic/Photoelectrocatalytic Oxidation of Nitrogen Oxides. *Trans. Tianjin Univ.* **2021**, *27*, 295–312. https://doi.org/10.1007/s12209-021-00293-9.
13. Cant, N.W.; Cole, J.R. Photocatalysis of the Reaction between Ammonia and Nitric Oxide on TiO_2 Surfaces. *J. Catal.* **1992**, *134*, 317–330. https://doi.org/10.1016/0021-9517(92)90231-6.
14. Bowering, N.; Walker, G.S.; Harrison, P.G. Photocatalytic Decomposition and Reduction Reactions of Nitric Oxide over Degussa P25. *Appl. Catal. B Environ.* **2006**, *62*, 208–216. https://doi.org/10.1016/j.apcatb.2005.07.014.
15. Malinowski, S.; Presečki, I.; Jajčinović, I.; Brnardić, I.; Mandić, V.; Grčić, I. Intensification of Dihydroxybenzenes Degradation over Immobilized TiO_2 Based Photocatalysts under Simulated Solar Light. *Appl. Sci.* **2020**, *10*, 7571. https://doi.org/10.3390/app10217571.
16. Grčić, I.; Marčec, J.; Radetić, L.; Radovan, A.-M.; Melnjak, I.; Jajčinović, I.; Brnardić, I. Ammonia and Methane Oxidation on TiO_2 Supported on Glass Fiber Mesh under Artificial Solar Irradiation. *Environ. Sci. Pollut. Res.* **2021**, *28*, 18354–18367. https://doi.org/10.1007/s11356-020-09561-y.
17. Grčić, I.; Papić, S.; Brnardić, I. Photocatalytic Activity of TiO_2 Thin Films: Kinetic and Efficiency Study. *Int. J. Chem. React. Eng.* **2018**, *16*, 20160153. https://doi.org/10.1515/ijcre-2016-0153.
18. NARVA BIO Vital®… Like Natural Sunglight. Available online: https://catalog.bailey.nl/webfiles/Catalogi/Narva/Narva_BIO_Vital_EN.pdf (accessed on 29 June 2024).
19. Navier-Stokes Equations. Available online: https://www.comsol.com/multiphysics/navier-stokes-equations (accessed on 25 May 2024).
20. Van Faassen, E. ; Vanin, A.F. Nitric Oxide Radicals and Their Reactions. In *Radical for Life: The Various Forms of Nitric Oxide*; Elsevier B.V.: Amsterdam, The Netherlands, 2007; ISBN 978-0444522368.
21. Ching, W.H.; Leung, M.; Leung, D.Y.C. Solar Photocatalytic Degradation of Gaseous Formaldehyde by Sol-Gel TiO_2 Thin Film for Enhancement of Indoor Air Quality. *Sol. Energy* **2004**, *77*, 129–135. https://doi.org/10.1016/j.solener.2004.05.012.
22. Li, G.; Zhang, D.; Yu, J.C.; Leung, M.K.H. An Efficient Bismuth Tungstate Visible-Light-Driven Photocatalyst for Breaking down Nitric Oxide. *Environ. Sci. Technol.* **2010**, *44*, 4276–4281. https://doi.org/10.1021/es100084a.
23. Dai, W.; Tao, Y.; Zou, H.; Xiao, S.; Li, G.; Zhang, D.; Li, H. Gas-Phase Photoelectrocatalytic Oxidation of NO via TiO_2 Nanorod Array/FTO Photoanodes. *Environ. Sci. Technol.* **2020**, *54*, 5902–5912. https://doi.org/10.1021/acs.est.9b07757.
24. Ai, Z.; Ho, W.; Lee, S.; Zhang, L. Efficient Photocatalytic Removal of NO in Indoor Air with Hierarchical Bismuth Oxybromide Nanoplate Microspheres under Visible Light. *Environ. Sci. Technol.* **2009**, *43*, 4143–4150. https://doi.org/10.1021/es9004366.
25. Shie, J.L.; Lee, C.H.; Chiou, C.S.; Chang, C.T.; Chang, C.C.; Chang, C.Y. Photodegradation Kinetics of Formaldehyde Using Light Sources of UVA, UVC and UVLED in the Presence of Composed Silver Titanium Oxide Photocatalyst. *J. Hazard. Mater.* **2008**, *155*, 164–172. https://doi.org/10.1016/j.jhazmat.2007.11.043.
26. Fermoso, J.; Sánchez, B.; Suarez, S. Air Purification Applications Using Photocatalysis. In *Nanostructured Photocatalysts*; Boukherroub, R., Ogale, S.B., Robertson, N., Eds.; Elsevier: Amsterdam, The Netherlands, 2020; pp. 99–128.
27. Grčić, I.; Radetić, L.; Miklec, K.; Presečki, I.; Leskovar, K.; Meaški, H.; Čizmić, M.; Brnardić, I. Solar Photocatalysis Application in UWWTP Outlets—Simulations Based on Predictive Models in Flat-Plate Reactors and Pollutant Degradation Studies with in Silico Toxicity Assessment. *J. Hazard. Mater.* **2024**, *461*, 132589. https://doi.org/10.1016/j.jhazmat.2023.132589.
28. Geng, Q.; Wang, H.; Chen, R.; Chen, L.; Li, K.; Dong, F. Advances and Challenges of Photocatalytic Technology for Air Purification. *Natl. Sci. Open* **2022**, *1*, 20220025. https://doi.org/10.1360/nso/20220025.
29. Chen, M.; Liu, Y. NO_x Removal from Vehicle Emissions by Functionality Surface of Asphalt Road. *J. Hazard. Mater.* **2010**, *174*, 375–379. https://doi.org/10.1016/j.jhazmat.2009.09.062.
30. Chen, M.; Chu, J. NO_x Photocatalytic Degradation on Active Concrete Road Surface—From Experiment to Real-Scale Application. *J. Clean. Prod.* **2011**, *19*, 1266–1272. https://doi.org/10.1016/j.jclepro.2011.03.001.
31. He, F.; Jeon, W.; Choi, W. Photocatalytic Air Purification Mimicking the Self-Cleaning Process of the Atmosphere. *Nat. Commun.* **2021**, *12*, 2528. https://doi.org/10.1038/s41467-021-22839-0.
32. Duan, Y.; Luo, J.; Zhou, S.; Mao, X.; Shah, M.W.; Wang, F.; Chen, Z.; Wang, C. TiO_2-Supported Ag Nanoclusters with Enhanced Visible Light Activity for the Photocatalytic Removal of NO. *Applied Catal. B Environ.* **2018**, *234*, 206–212. https://doi.org/10.1016/j.apcatb.2018.04.041.
33. Jiang, Q.; Qi, T.; Yang, T.; Liu, Y. Ceramic Tiles for Photocatalytic Removal of NO in Indoor and Outdoor Air under Visible Light. *Build. Environ.* **2019**, *158*, 94–103. https://doi.org/10.1016/j.buildenv.2019.05.014.
34. Cassano, A.E.; Alfano, O.M. Reaction Engineering of Suspended Solid Heterogeneous Photocatalytic Reactors. *Catal. Today* **2000**, *58*, 167–197. https://doi.org/10.1016/S0920-5861(00)00251-0.
35. Esteban Duran, J.; Mohseni, M.; Taghipour, F. Computational Modeling of UV Photocatalytic Reactors: Model Development, Evaluation, and Application. *Water Qual. Res. J. Canada* **2015**, *50*, 21–33. https://doi.org/10.2166/wqrjc.2014.031.
36. Baetens, D.; Schoofs, K.; Somers, N.; Denys, S. A Brief Review on Multiphysics Modelling of the Various Physical and Chemical Phenomena Occurring in Active Photocatalytic Oxidation Reactors. *Curr. Opin. Green Sustain. Chem.* **2023**, *40*, 100764. https://doi.org/10.1016/j.cogsc.2023.100764.

37. Roegiers, J.; van Walsem, J.; Denys, S. CFD- and Radiation Field Modeling of a Gas Phase Photocatalytic Multi-Tube Reactor. *Chem. Eng. J.* **2018**, *338*, 287–299. https://doi.org/10.1016/j.cej.2018.01.047.
38. Pareek, V.K.; Adesina, A.A. Light Intensity Distribution in a Photocatalytic Reactor Using Finite Volume. *AIChE J.* **2004**, *50*, 1273–1288. https://doi.org/10.1002/aic.10107.
39. Boyjoo, Y.; Ang, M.; Pareek, V. Some Aspects of Photocatalytic Reactor Modeling Using Computational Fluid Dynamics. *Chem. Eng. Sci.* **2013**, *101*, 764–784. https://doi.org/10.1016/j.ces.2013.06.035.
40. Janczarek, M.; Kowalska, E. Computer Simulations of Photocatalytic Reactors. *Catalysts* **2021**, *11*, 198. https://doi.org/10.3390/catal11020198.
41. Trujillo, F.J.; Safinski, T.; Adesina, A.A. CFD Analysis of the Radiation Distribution in a New Immobilized Catalyst Bubble Column Externally Illuminated Photoreactor. *J. Sol. Energy Eng. Trans. ASME* **2007**, *129*, 27–36. https://doi.org/10.1115/1.2391013.
42. Moreno-SanSegundo, J.; Casado, C.; Marugán, J. Enhanced Numerical Simulation of Photocatalytic Reactors with an Improved Solver for the Radiative Transfer Equation. *Chem. Eng. J.* **2020**, *388*, 124183. https://doi.org/10.1016/j.cej.2020.124183.
43. Satuf, M.L.; Brandi, R.J.; Cassano, A.E.; Alfano, O.M. Scaling-up of Slurry Reactors for the Photocatalytic Degradation of 4-Chlorophenol. *Catal. Today* **2007**, *129*, 110–117. https://doi.org/10.1016/j.cattod.2007.06.056.
44. van Walsem, J.; Roegiers, J.; Modde, B.; Lenaerts, S.; Denys, S. Proof of Concept of an Upscaled Photocatalytic Multi-Tube Reactor: A Combined Modelling and Experimental Study. *Chem. Eng. J.* **2019**, *378*, 122038. https://doi.org/10.1016/j.cej.2019.122038.
45. van Walsem, J.; Verbruggen, S.W.; Modde, B.; Lenaerts, S.; Denys, S. CFD Investigation of a Multi-Tube Photocatalytic Reactor in Non-Steady-State Conditions. *Chem. Eng. J.* **2016**, *304*, 808–816. https://doi.org/10.1016/j.cej.2016.07.028.
46. Imoberdorf, G.E.; Irazoqui, H.A.; Alfano, O.M.; Cassano, A.E. Scaling-up from First Principles of a Photocatalytic Reactor for Air Pollution Remediation. *Chem. Eng. Sci.* **2007**, *62*, 793–804. https://doi.org/10.1016/j.ces.2006.10.004.